

Towards High Performance Li–S Batteries via Sulfonate-Rich COF-Modified Separator

Jie Xu, Shuhao An, Xianyu Song, Yongjie Cao, Nan Wang, Xuan Qiu, Yu Zhang, Jiawei Chen, Xianli Duan, Jianhang Huang, Wei Li,* and Yonggang Wang*

Lithium–sulfur (Li–S) batteries are held great promise for next-generation high-energy-density devices; however, polysulfide shuttle and Li-dendrite growth severely hinders their commercial production. Herein, a sulfonate-rich COF (SCOF-2) is designed, synthesized, and used to modify the separator of Li–S batteries, providing a solution for the above challenges. It is found that the SCOF-2 features stronger electronegativity and larger interlayer spacing than that of none/monosulfonate COFs, which can facilitate the Li⁺ migration and alleviate the formation of Li-dendrites. Density functional theory (DFT) calculations and in situ Raman analysis demonstrate that the SCOF-2 possesses a narrow bandgap and strong interaction on sulfur species, thereby suppressing self-discharge behavior. As a result, the modified batteries deliver an ultralow attenuation rate of 0.047% per cycle over 800 cycles at 1 C, and excellent anti-self-discharge performance by a low-capacity attenuation of 6.0% over one week. Additionally, even with the high-sulfur-loading cathode (3.2–8.2 mg_s cm⁻²) and lean electrolyte (5 μL mg_s⁻¹), the batteries still exhibit ≈80% capacity retention over 100 cycles, showing great potential for practical application.

secondary batteries.^[1] However, due to the limited energy density (≈387 Wh kg⁻¹) of currently used Li-ion batteries (LIBs), they have gradually been unable to meet the requirements of practical applications. Benefiting from the characteristics of sulfur substance that with environmental friendliness, natural abundance, low cost, and high theoretical energy density (2600 Wh kg⁻¹), lithium–sulfur (Li–S) batteries offer great potentials for the next-generation energy storage systems.^[2] The working mechanism of S-cathode is based on the redox reaction between elemental sulfur and Li-ions to produce long-chain and short-chain lithium polysulfides (LiPSs).^[3] Generally, the soluble polysulfides (i.e., the polysulfide anions and the molecular LiPSs) can shuttle through the macroporous polyolefin separator, leading to the irreversible loss of active substances, self-discharge behavior,

and severe capacity attenuation.^[4,5] Moreover, the polysulfide passing from the cathodic region could accumulate on the anode surface and further reduce to short-chain Li₂S₂/Li₂S, which can corrode the solid electrolyte interphase (SEI) and give rise to dendrite growth.^[6] All of the above issues give formidable challenges to realize high-performance Li–S batteries with good cyclic stability and a long lifespan.

Covalent organic frameworks (COFs), which are characterized by lightweight elements, tunable chemical nature, and robust chemical/thermal stability, providing opportunities to construct task-specific materials for challenging Li–S batteries.^[7] The encapsulation of sulfur into the channel of COF is one of the most widely used strategies, of which LiPSs could be restricted within the cathodic area.^[8] However, the soluble LiPSs cannot be fully constrained and inevitably dissolved into the solvent, accompanying by shuttle behavior over long-term cycles. Beyond that, the sulfur components could also be polymerized on the COF matrix through covalent bonding (i.e., S_NAr reaction), which allows fundamental investigation over the interplay between COF host and polymerized sulfur.^[9] Nevertheless, the poor conductivity of COF reduces the utilization rate of sulfur cathode. Owing to the advantages of intrinsically ordered pores, tunable building blocks, and selective permeability of Li ions, the research interest has shifted to separator modification.^[10] In 2018, Wang and co-workers^[11a] proposed a COF-rGO double-layer membrane acting as ionic sieves


1. Introduction

With the huge demand for portable devices and electric vehicles, it is highly urgent to develop high-energy-density

J. Xu, Y. Cao, N. Wang, X. Qiu, Y. Zhang, J. Chen, J. Huang, W. Li, Y. Wang
Department of Chemistry and Shanghai Key Laboratory of Molecular Catalysis and Innovative Materials
Institute of New Energy
iChEM (Collaborative Innovation Center of Chemistry for Energy Materials)
Fudan University
Shanghai 200433, China
E-mail: weilichem@fudan.edu.cn; ygwang@fudan.edu.cn

S. An
Key Laboratory for Advanced Materials and School of Chemistry and Molecular Engineering
East China University of Science and Technology
Shanghai 200237, China

X. Song, X. Duan
Chongqing Key Laboratory of Water Environment Evolution and Pollution Control in Three Gorges Reservoir
School of Environmental and Chemical Engineering
Chongqing Three Gorges University
Wanzhou 404020, China

 The ORCID identification number(s) for the author(s) of this article can be found under <https://doi.org/10.1002/adma.202105178>.

DOI: 10.1002/adma.202105178

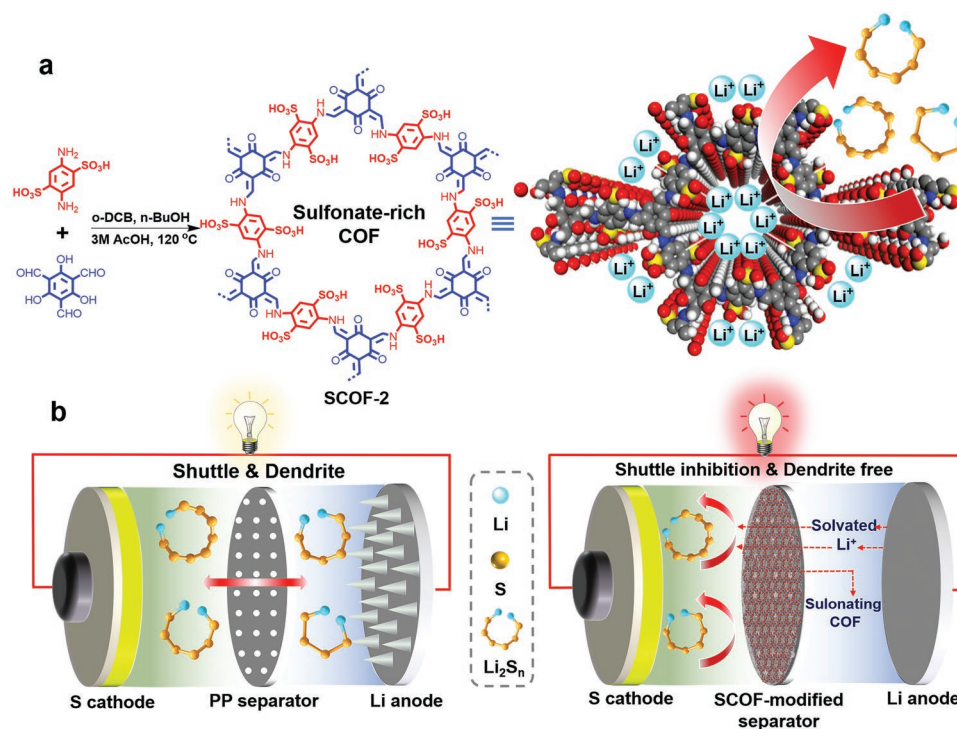
to inhibit the shuttle effect of polysulfide. Then, Guo and co-workers^[11b] reported a benzobisthiadiazole (BBT)-based COF modified separator for adsorbing the undesired LiPSs through the interaction between BBT active site and LiPSs. Moreover, Sun and co-workers^[12] investigated a lithiated triazole-based COF for chemically trapped polysulfides and simultaneously increased the conduction of Li⁺. However, the polysulfidic anion is a kind of Lewis base that different from the molecular LiPSs, which cannot be entrapped completely by the low-pole COF skeleton. Besides, the solvated Li⁺ that with a large space size generally brings inferior mobility in a densely stacked COF layer.^[13] To construct a functional COF that with strong polarity, large layer spacing, and narrow bandgap for blocking polysulfide species and synchronously regulating the transportation of Li⁺/e⁻ is essential but still challenging.

Herein, we design and synthesize a dual-sulfonate COF (denoted as SCOF-2) and use it to modify the separator of Li-S batteries to provide a solution for the above challenges. The SCOF-2 tethered with the concentrated sulfonic group could act as an ionic sieve for repelling polysulfide anions, adsorbing molecular LiPSs, and simultaneously facilitating Li⁺ migration (Scheme 1a). Compared with that none/mono-sulfonate COFs, it is found that the SCOF-2 features stronger electronegativity and larger interlayer spacing, which can not only block the polysulfides migration but also alleviate the formation of Li-dendrites. DFT calculations and in-situ Raman analysis demonstrate that the SCOF-2 possesses a narrow bandgap and strong interaction on sulfur species, thereby suppressing self-discharge behavior. Accordingly, the SCOF-2 modified batteries deliver a high rate capacity of 479 mAh g⁻¹ at 5 C current, an

ultralow attenuation rate of 0.047% per cycle over 800 cycles at 1 C, and an excellent anti-self-discharge behavior by a low capacity attenuation of 6.0% over one week rest. Besides, a reversible capacity of 4.92 mAh cm⁻² and 81.2% capacity retention over 100 cycles are achieved under the conditions of 8.2 mg_s cm⁻² sulfur loading and lean electrolyte (5 μL mg⁻¹), overwhelming most other COF materials used in Li-S batteries.

2. Results and Discussion

As illustrated in Scheme 1a, the SCOF-2 was synthesized from the condensation reaction of 2,5-diaminobenzene-1,4-disulfonic acid and 2,4,6-trihydroxybenzene-1,3,5-tricarbaldehyde based on conventional Schiff-base reaction.^[14] By changing the sulfonated building block with benzene-1,4-diamine or 2,5-diaminobenzenesulfonic acid, the counterparts of none-sulfonate COF (TpPa-COF) and monosulfonate COF (SCOF-1) were also synthesized for comparison (Scheme S1, Supporting Information). In comparison with the pristine PP separator, the electronegative SCOF may block undesirable polysulfide species and simultaneously enable selective permeability of Li⁺, thereby preventing the Li anode from being corroded (Scheme 1b). The crystalline structure of COFs is firstly investigated by the powder X-ray diffraction (PXRD) and theoretical structural simulations. The experimental PXRD results indicate that SCOF-2 has two well-reserved peaks at 4.55° and 26.77°, corresponding to the (100), and (001) facets, respectively, which confirms the eclipsed stacking model (Figure 1a). After Pawley refinement, the unit cell parameters are $a = b = 22.85 \text{ \AA}$, and



Scheme 1. a) Schematic synthesis of the sulfonated COFs, selective permeability of Li⁺, and the blocking of polysulfides in Li-S batteries. b) Graphic comparison of the batteries with different separators: the battery with polypropylene (PP) separator shows shuttle effect and dendrite growth (left), while the SCOF-modified battery shows shuttle inhibition and dendrite-free (right).

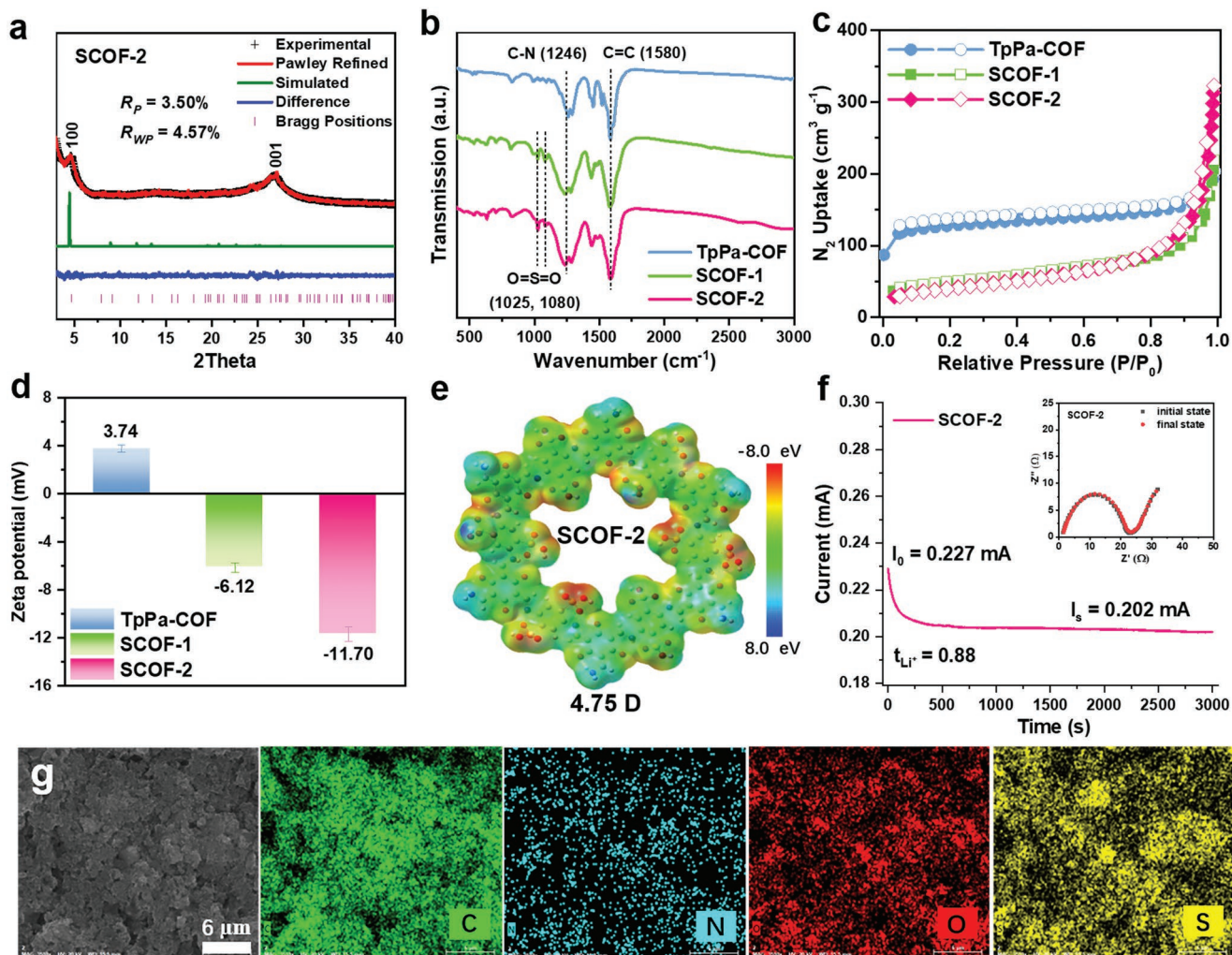


Figure 1. a) PXRD patterns of SCOF-2. b) FT-IR spectra, c) N_2 adsorption–desorption curves, and d) zeta potential value of various COF materials. e) Electrostatic potential distributions and dipole moments of SCOF-2 (D is short for Debye). f) Chronoamperometric curve, inset is EIS plots of the symmetric cell. g) SEM images and the corresponding elemental mapping images of SCOF-2 modified separator.

$c = 4.61 \text{ \AA}$ with satisfied factors of $R_p = 3.50\%$ and $R_{wp} = 4.57\%$. In addition, the PXRD patterns of TpPa-COF and SCOF-1 also exhibit characteristic peaks and decent crystallographic structures, which is similar to the reported study (Figures S1 and S2, Supporting Information).^[14b] Admittedly, the peak width at half height of SCOF-2 is larger than that of TpPa-COF and/or SCOF-1, implying the decreased crystallinity for SCOF-2. Such phenomenon is majorly attributed to the large steric hindrance from dense sulfonic groups, which induces inferior π - π stacking between successive COF layers and impaired crystallinity. Nevertheless, the SCOF-2 features a larger interlayer spacing ($c = 4.61 \text{ \AA}$) than those of TpPa-COF (3.39 \AA) and SCOF-1 (4.29 \AA), which may induce fast Li^+ migration across COF interlayer.

Further, the characteristic peak of $\approx 183.2 \text{ ppm}$ in the solid-state ^{13}C NMR spectra corresponds to the chemical shift of keto-form carbonyl carbon for SCOF-2 (Figure S3, Supporting Information), as well as the similar chemical shifts for TpPa-COF and SCOF-1 at 183.9 and 183.6 ppm, respectively (Figures S4 and S5, Supporting Information). Moreover, FT-IR collections

show the characteristic peaks at 1246 and 1580 cm^{-1} for three COFs, which ascribe to the C–N and C=C stretching vibration bands (Figure 1b). As for the SCOFs, the newly formed peaks at 1025 and 1080 cm^{-1} are belonged to the stretching band of S=O, indicating the existence of sulfonic groups. Thermogravimetric analysis shows that all COFs display favorable thermal stability under nitrogen atmosphere, and the weight is retained 41–47% even the temperature up to 800 $^{\circ}C$ (Figure S6, Supporting Information). According to scanning electron microscopy (SEM) and transmission electron microscopy (TEM) observations, the morphologies of TpPa-COF and SCOF-2 are composed of nanoparticles and short nanofibers, while the SCOF-1 shows relatively long and smooth nanofiber morphology (Figures S7 and S8, Supporting Information). The N_2 adsorption isotherms show that the TpPa-COF adopt both type I and IV isotherms, indicating the coexistence of micropores and mesopores. In contrast, the SCOF-1 and SCOF-2 show a typical type IV isotherm, showing the presence of mesopores (Figure 1c). The Brunauer–Emmett–Teller (BET) surface area of TpPa-COF is calculated to be 410 $m^2 g^{-1}$ accompanying with an

ordered pore size of 1.65 nm, while the SCOF-1 and SCOF-2 exhibit smaller surface area of 161 and 144 m² g⁻¹ and mainly show mesoporous distributions (Figure S9, Supporting Information). Such phenomenon is mainly due to the self-exfoliation property of SCOFs, which results in an increase of interlayer spacing and a decrease of molecular packing pores.

The surface charge property of COFs is further investigated by zeta potential test (Figures S10–S12, Supporting Information). As shown in Figure 1d, the TpPa-COF presents a positive value of 3.74 mV, while SCOF-1 and SCOF-2 exhibit negative values of -6.12 and -11.7 mV, respectively. The negative potential value indicates the electronegativity nature of SCOF-1 and SCOF-2, which arises from the sulfonic groups. Accordingly, the SCOF-2 with strong electronegativity could repel polysulfide anions through electrostatic repulsion interaction. As the electrostatic potential distribution shown in Figure 1e, the sulfonic group in SCOF-2 presents intense electron density (red color region), which could form the nucleophilic interaction toward LiPSs.^[15] That is to say, the SCOF-2 could block polysulfides via both electrostatic repulsion (i.e., repelling polysulfide anions) and chemical trapping (i.e., adsorbing molecular LiPSs), which will be confirmed by later experiments and DFT calculation. Compared with TpPa-COF (0 D), the SCOF-1 and SCOF-2 exhibit increased dipole moment values of 9.44 D and 4.75 D, respectively (Figure S13, Supporting Information). The dipole moment of SCOF-1 is larger than that of SCOF-2, which may be the asymmetric structure of the monosulfonic group resulting in enhanced distance between positive and negative charge centers.^[16]

Subsequently, the COF-modified separators were prepared with a thin layer ($\approx 6 \mu\text{m}$) and a low COF loading of 0.15 mg cm⁻² (Figure S14, Supporting Information). The physicochemical parameters including ionic conductivity and Li⁺ transference number of modified separator were evaluated, respectively.^[17a] Specifically, the ionic conductivity of SCOF-2 is determined to be 2.06 mS cm⁻¹, which is higher than TpPa-COF (0.83) and SCOF-1 (1.05), indicating that the sulfonate-rich interface could enable efficient Li-ion conduction (Figure S15, Supporting Information). Similar to the ionic conductivity, the SCOF-2 modified separator (Figure 1f) exhibits a higher Li⁺ transference number of 0.88 than that of TpPa-COF (0.63) and SCOF-1 (0.74), respectively (Figure S16, Supporting Information). The ionic conductivity and Li⁺ transference number of pristine Celgard separator are 0.70 mS cm⁻¹ and 0.61, respectively, which are inferior to these COF-modified separators (Figure S17, Supporting Information). Previous report demonstrated that the sulfonate groups with electronegativity can simultaneously facilitate access by the electrolyte to promote ion pair dissociation and increase the mobility of Li⁺.^[17b] Accordingly, SCOF-2 modified separator shows the higher Li⁺ transference number because SCOF-2 possesses both abundant sulfonate groups and large interlayer space. Besides, the elemental mapping images (Figure 1g) show that SCOF-2 is uniformly coated on the surface of PP separator and forms a dense layer to block the migration of polysulfides.

The electrochemical performance is investigated with the coin cell by pairing the S/CB cathode (75% content, 1.3–1.5 mg_s cm⁻²), COF-modified separator, and Li anode. Cyclic voltammetry (CV) show that the SCOF-2 modified cell

possesses a narrower polarization voltage (0.414 V) than that of TpPa-COF (0.571 V) and SCOF-1 (0.450 V), indicating fast kinetics of redox reaction (Figure S18, Supporting Information).^[18] Further, the diffusion coefficient of Li⁺ (D_{Li^+}) is also measured. Given the CV curves in Figure 2a–c, the cathodic and anodic scans typically include two reduction peaks (peak I_{R1}, I_{R2}) and two oxidation peaks (peak I_{O1}, I_{O2}), respectively, and the peak currents under various scan rates are highly relevant with the linear fitting results (Figure S19, Supporting Information).^[19,20] In particular, the D_{Li^+} of peak I_{R2} is calculated to be $1.32 \times 10^{-7} \text{ cm}^2 \text{ s}^{-1}$ for SCOF-2 modified cell, which is 2.6 and 4.3 times higher than those of SCOF-1 and TpPa-COF, respectively, which is mainly due to the enhanced interlayer spacing of SCOF-2 facilitating the migration of Li⁺. In addition, it is found that the SCOF-2 exhibits higher catalytic activity for the conversion of lithium polysulfide than SCOF-1 and TpPa-COF (Figure S20, Supporting Information).

Afterwards, the TpPa-COF modified cell shows an initial discharge capacity of 910 mAh g⁻¹ at the current of 0.1 C and a relatively low capacity of 300 mAh g⁻¹ at upper discharge plateau (Figure 2d). In contrast, the capacities increase to 1057 and 1235 mAh g⁻¹ for SCOF-1 and SCOF-2 modified cells, respectively, and present enhanced capacities at upper discharge plateau indicating the higher utilization rate of the sulfur cathode.^[21] In particular, the SCOF-2 modified cell delivers the highest capacity of 356 mAh g⁻¹ at the upper discharge plateau, as well as the narrowest polarization voltage of 0.10 V between the discharge and charge curves. As for the lower discharge plateau ($\approx 2.1 \text{ V}$), the TpPa-COF, SCOF-1, and SCOF-2 deliver 610, 713, and 879 mAh g⁻¹, respectively. The largest capacity obtained for SCOF-2 at the lower discharge plateau indicates the high conversion rate from Li₂S₄ to solid Li₂S₂/Li₂S. Moreover, rate performance under the current from 0.1 to 5 C shows that both SCOF-1 and SCOF-2 exhibit higher capacities than TpPa-COF modified cell (Figure 2e). The corresponding charge/discharge curves of these cells at different rates are shown in Figure S21 (Supporting Information), where it can be detected that the SCOF-2 modified cell exhibits the best rate capability. Furthermore, the influence of SCOF-2 modified separator on the performance of Li anode was studied by testing the Li||Li symmetric cell. As the rate performance shown in Figure 2f, the SCOF-2 exhibits narrower voltage hysteresis than pristine PP separator. Particularly, the cell with PP separator shows huge voltage hysteresis ($\geq 300 \text{ mV}$) at the current density of 5 mA cm⁻², while the SCOF-2 possesses a stable and small voltage hysteresis of 42 mV (see Figure S22 (Supporting Information) for the enlargement of Figure 2f). Beyond that, the long-term cycling test (Figure 2g) discloses that the cell with SCOF-2 manifests a low and stable polarization behavior ($\approx 10 \text{ mV}$), demonstrating that the dendrite growth is remarkably inhibited.

Then, the battery was disassembled after rate cycling to practically analyze the effect of COF-modified separator on Li anode. Obviously, it is observed that many bulk particles and cracks on the anode surface for TpPa-COF modified cell (Figure 3a), and the corresponding energy dispersive spectroscopy (EDS) disclosed that there is 16.10% sulfur content on its surface (Figure S23, Supporting Information). In contrast, the cells with SCOF-1 and SCOF-2 have an intact and smooth anode surface (Figure 3b,c), which are detected with low sulfur

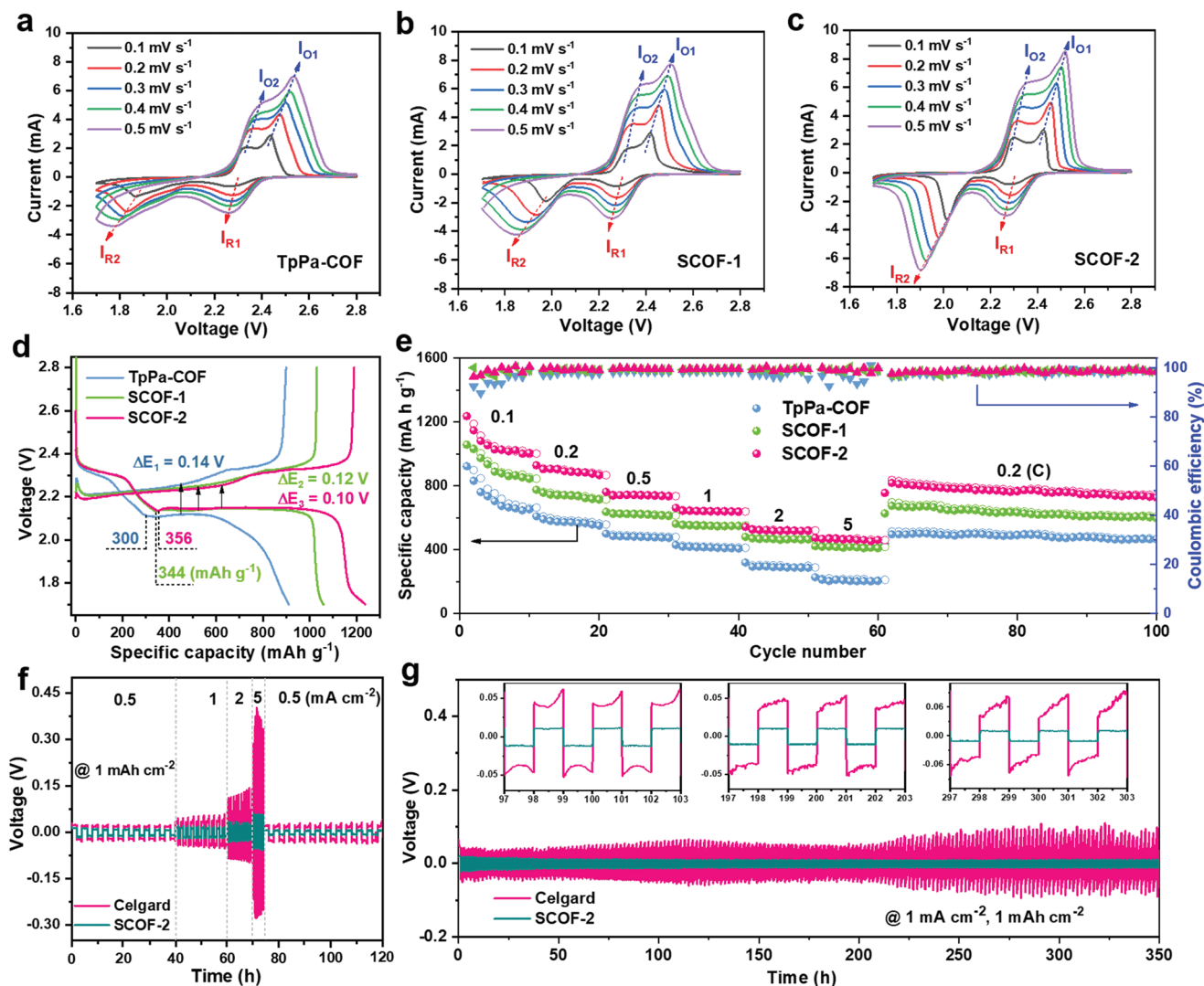


Figure 2. CV profiles at different scan rates with a) TpPa-COF, b) SCOF-1, and c) SCOF-2 modified separator. The charge–discharge voltage profile at the current of d) 0.1 C, and e) rate performance of COF-modified separator. f) Rate performance and g) cycling stability of Li||Li symmetric cells with Celgard and SCOF-2 modified separators (insets are the local enlargement of selected cycles).

signals of 9.04% and 5.12%, respectively. In addition, a dense and bulky Li layer could be observed from the cross-sectional images, the thickness of 180, 130, and 70 μm was obtained for TpPa-COF, SCOF-1, and SCOF-2, respectively (Figure 3d–f). The increased thickness is mainly ascribed to that the cross-over polysulfides interact with the Li metal and finally reduce to solid-state $\text{Li}_2\text{S}_2/\text{Li}_2\text{S}$ on the anode surface.^[22] As illustrated in Figure 3g, the none-sulfonate COF (TpPa-COF) may possess a little chemical interaction with polysulfides and bring about dense passivation and corrosion layer on the surface of anode, which is the major reason for the formation of Li dendrite over long-term cycling. Moreover, the monosulfonate COF (SCOF-1) has the inferior ability of polysulfide blocking and give rise to the uneven distribution of Li-ion flux and anode corrosion after long-term cycling (Figure 3h). Particularly, the dual-sulfonate COF (SCOF-2) possesses a strong electronegative ability for blocking polysulfides and achieves a uniform Li-ion distribution, resulting in a stable SEI layer and dendrite-free anode

(Figure 3i). Therefore, the SCOF-2 modified separator could serve as an efficient ionic sieve to uniformly filter and redistribute the Li-ion flux and regulate the Li plating/stripping process.

To deeply probe the role of sulfonate COF in blocking the shuttle of polysulfides, in-situ Raman spectroscopy was conducted to detect the polysulfides shuttling to the anode side in real-time.^[23] As shown in Figure 4a–d, the time-resolved Raman contour maps and selected Raman signals of TpPa-COF or SCOF-2 modified cells at different discharge states are compared, respectively. For the cell with TpPa-COF-modified separator, signals of S_8^{2-} (characteristic peaks at 150, 219, and 478 cm^{-1}) are detected at the beginning of discharge (2.33 V), indicating that the long-chain Li_2S_8 is formed and shuttled. Following the discharge process, the three main peaks of S_8^{2-} slightly decrease, and peaks at around 300 and 400 cm^{-1} arise at the same time, which are belonged to the characteristics S_4^{2-} , S_5^{2-} , and S_6^{2-} , respectively.^[24] Moreover, the prominent

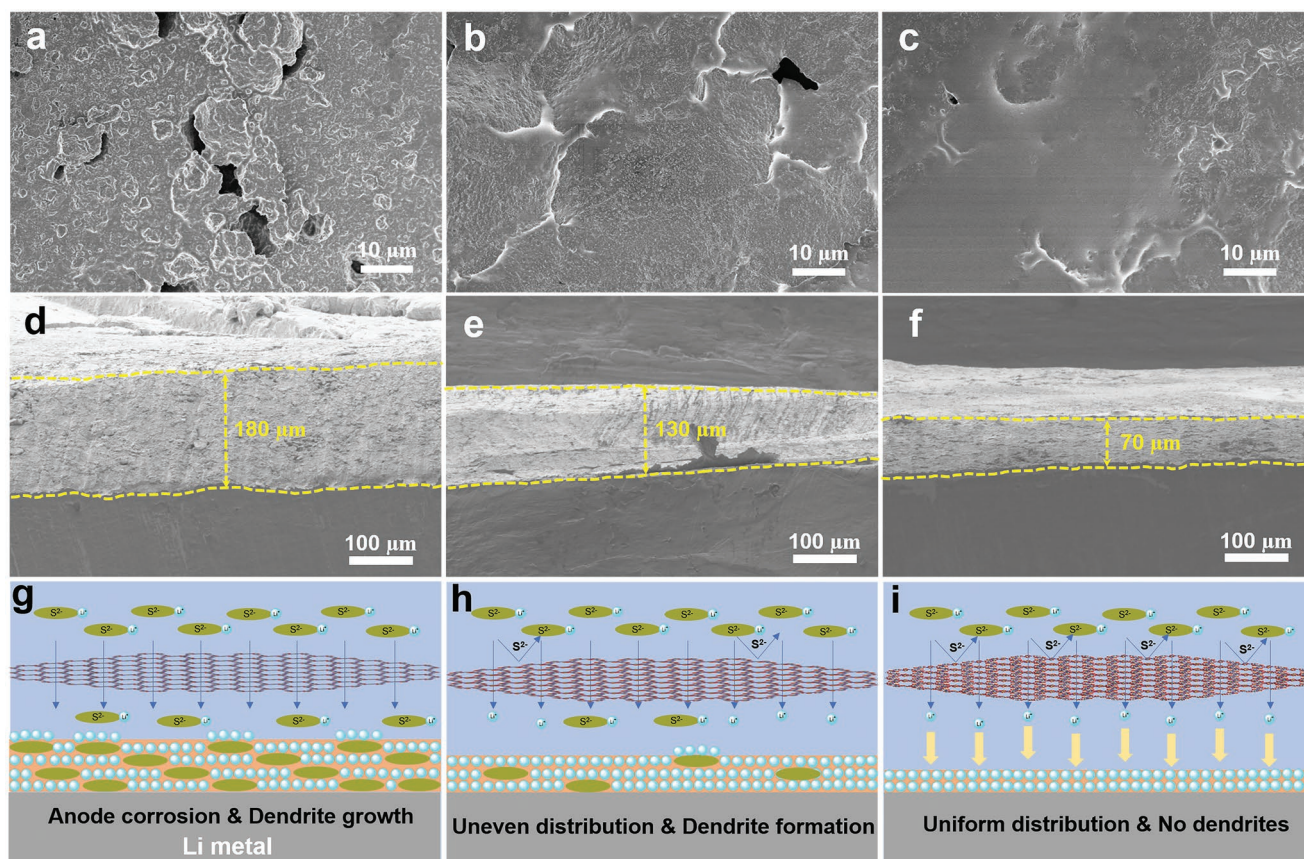


Figure 3. a–c) Top-view and d–f) cross-sectional SEM images of Li anode, a,d) for TpPa-COF, b,e) for SCOF-1, and c,f) for SCOF-2, respectively. Schematic illustration of cycled Li behaviors with g) TpPa-COF, h) SCOF-1, i) SCOF-2 modified separators, respectively.

characteristic peaks of S_4^{2-} , S_5^{2-} , S_6^{2-} , and S_8^{2-} are still remained during the charge process (Figure S24, Supporting Information), suggesting polysulfides shuttling and the irreversible loss of sulfur species. In contrast, the cell containing SCOF-2 modified separator shows tiny Raman signals of polysulfides in both the discharge and charge processes, demonstrating that the migration of polysulfides is effectively blocked.

Additionally, the elemental compositions on the surface of cycled COF-modified separators were analyzed by X-ray photoelectron spectroscopy (XPS). It should be noted that all the separators are tested after the charge process. As shown in Figure 4e, all S 2p bands are decoupled into two sub-peaks (S $2P_{1/2}$ & S $2P_{3/2}$) with an energy gap of 1.18 eV. Specifically, the binding energies at 163.97, 163.20, and 161.78 eV are indexed to the bands of S_8 , bridging S–S, and terminal S–Li, respectively.^[19] It is found that sulfur species on different COF-modified separators exhibit various valence states, implying that the redox reversibility of polysulfides is different. Thereafter, the band areas of sulfur species are quantified to facilitate further analysis (Figure S25, Supporting Information). As for the TpPa-COF modified cell, the terminal S–Li band area (41.2%) is larger than those of bridging S–S (35.8%) and S_8 (23%), which indicates that many Li_2S_2/Li_2S did not oxidize to S_8 after full charge. After the modification with SCOF-1, the conversion rate of Li_2S_2/Li_2S to S_8 is increased, and the main band change to bridging S–S (36.4%) and S_8 (35.5%). In particular, the

dominant substances on SCOF-2 surface turn to be S_8 (66.4%), demonstrating that SCOF-2 can greatly promote the conversion of polysulfides. Besides, three sub-peaks at 56.13, 55.42, and 55.03 eV in Li 1s spectrum of TpPa-COF sample correspond to the Li–F, Li_2S_n , and Li–O bonding types (Figure 4f). In comparison, the peaks shift to high binding energy regions when with SCOF-1 or SCOF-2 modified separator, indicating the enhanced oxidation state of Li species. Especially, the SCOF-2 has the largest Li–O bonding areas (26.8%), which is probably due to the sulfonic group bringing about strong interaction with LiPSs.

Moreover, DFT calculations were applied to detect the active site and interaction energy of SCOFs toward polysulfide. Generally, the lowest unoccupied molecular orbital (LUMO) has the characteristics of electrons initially filled and extracted, which signifies the most active site for redox reaction.^[25] As shown in Figure 4g, the LUMO and HOMO configurations of TpPa-COF are delocalized on the whole skeleton, while SCOF-1 and SCOF-2 show more concentrated configurations and the LUMO configuration is mainly concentrated in the benzene-sulfonic group signifying the active site. Accordingly, the narrowest bandgap of 2.45 eV is obtained for SCOF-2 suggesting the enhanced electron conductivity, which is favorable for the conversion of intercepted polysulfides. It is well known that the soluble polysulfides mainly include the polysulfide anions (e.g., S_4^{2-} , S_6^{2-} , and S_8^{2-}) and molecular LiPSs (e.g., Li_2S_n ,

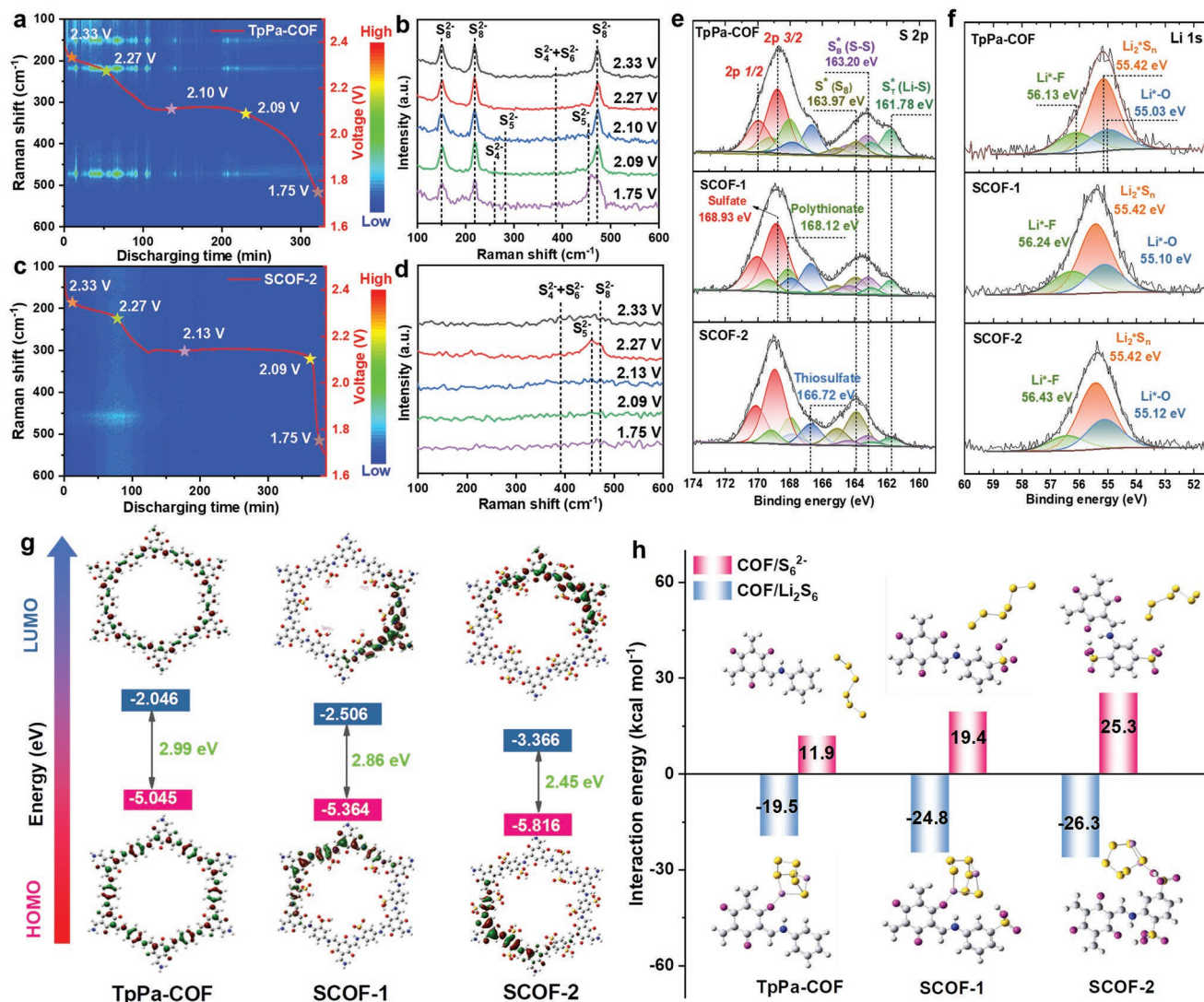


Figure 4. Time-resolved Raman spectra at 0.10 C of the discharge process and Raman signals of the batteries at different voltage states with a,b) TpPa-COF and c,d) SCOF-2-modified separators, respectively. XPS spectra of e) S 2p and f) Li 1s with different COF-modified separators at charged state. g) The lowest unoccupied molecular orbital (LUMO) and the highest occupied molecular orbital (HOMO) of various COF skeletons. h) Interaction between sulfur species (S_6^{2-} and Li_2S_6) and various COF monomers.

$4 \leq n \leq 8$).^[26] Here, the S_6^{2-} and Li_2S_6 as representative polysulfides are selected to investigate the interaction with COFs. As shown in Figure 4h, the interaction energy between COFs and S_6^{2-} exhibits a positive energy value indicating the electrostatic repulsion between COF and polysulfide anions. Specifically, an energy value of 11.9 kcal mol⁻¹ is obtained for the TpPa-COF monomer toward S_6^{2-} , while the energy increases to 19.4 and 25.3 kcal mol⁻¹ for SCOF-1 and SCOF-2 monomers, respectively, implying the increased repulsion ability of SCOFs. Beyond that, the interaction energy between COF monomer and Li_2S_6 shows a negative value, suggesting the binding behavior between COF and LiPSs. Compared with the TpPa-COF, SCOFs present increased binding energies, and the SCOF-2 shows the largest binding energy of -26.3 kcal mol⁻¹, which is mainly induced by the Lewis acid-base interaction between the sulfonic group and electron-deficient lithium atom of LiPSs.^[21] The interaction between SCOF and Li_2S_6 was further verified by

visual adsorption experiment and corresponding UV-vis analysis (Figure S26, Supporting Information). According to the DFT calculation, the SCOF-2 modified separator can block the undesired polysulfides shuttle in both the ways of electrostatic repulsion (i.e., repelling polysulfide anions) and chemical trapping (i.e., adsorbing molecular LiPSs), which is illustrated by Figure S27 in the Supporting Information.

One of the most grievous problems in Li-S batteries is the self-discharge behavior, which can result in the decrease of open-circuit potential (OCP) and cyclability.^[27] Hence, the anti-self-discharge ability is an important descriptor to evaluate the practical performance of Li-S batteries. As shown in Figure S28 in the Supporting Information, the batteries with different COF-modified separators are compared by the attenuation of OCP over 120 h standing, of which the SCOF-2 possesses the highest OCP value. Furthermore, the batteries discharged to 2.1 V at 10th cycle and rested for one week (Figure 5a).

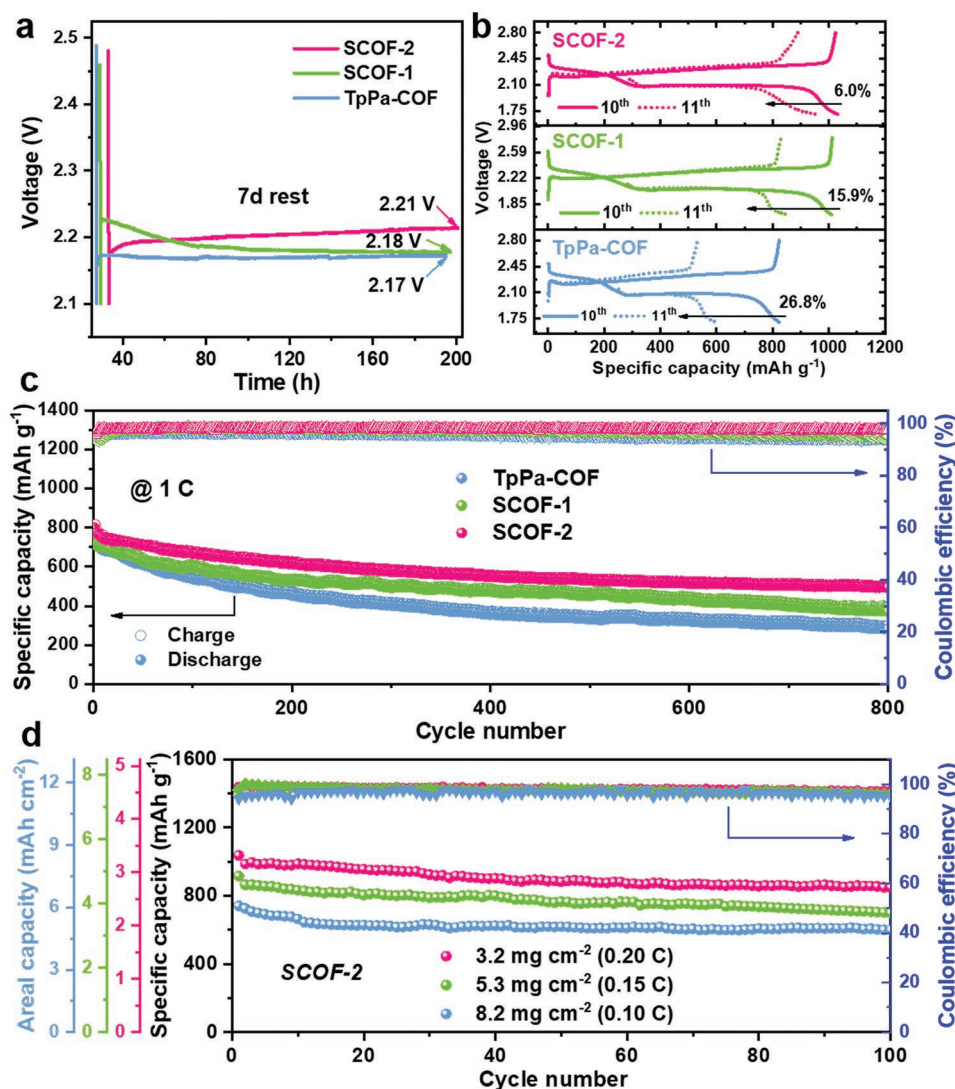


Figure 5. Comparison of electrochemical performance. a) Self-discharge behavior over 7 d rest. b) Comparison of capacity retention after rest, solid line is 10th cycle, dash line is 11th cycle. c) Long-term cycling at 1 C over 800 cycles. d) Cycling performance with S/CNT cathode under various sulfur loading of 3.2, 5.3, and 8.2 mg cm⁻², respectively.

Specifically, the TpPa-COF modified cell maintains a low final potential of 2.17 V and experiences a high capacity loss of 26.8% (150 mAh g⁻¹) that relative to the 10th discharge capacity (Figure 5b). In the case of SCOF-1, it shows a potential of 2.18 V after rest, while it still suffers from a relatively high capacity loss of 15.9% (120 mAh g⁻¹). Surprisingly, the SCOF-2 based cell exhibits a high potential of 2.21 V and simultaneously has a low capacity loss of 6.0% (65 mAh g⁻¹), indicating an excellent anti-self-discharge performance. In the subsequent cycles, the battery with SCOF-2 can still maintain stable cycle performance (Figure S29, Supporting Information), while the batteries with SCOF-1 and TpPa-COF manifest rapid capacity attenuation. These results validate that the sulfonate-rich COF modified cell has a strong ability to alleviate the self-discharge behavior.

Other factors including long-term cycling stability, high-sulfur loading, and lean electrolyte should also be critically considered in practical application.^[28] The cycling performances

over 800 cycles at 1 C were investigated (Figure 5c). The SCOF-2 initially delivers a decent capacity of 795 mAh g⁻¹ and maintains a reversible capacity of 497 mAh g⁻¹ after 800 cycles, which accompanies a low attenuation rate of 0.047% per cycle and a favorable average coulombic efficiency of 98.9%. In contrast, the TpPa-COF and SCOF-1 modified cells show low capacities and rapid decay during cycling (Figure S30, Supporting Information), fading from 739 to 282 mAh g⁻¹ and 745 to 372 mAh g⁻¹, respectively. Meanwhile, an obvious decrement of coulombic efficiencies for SCOF-1 (96.3%) and TpPa-COF (94.2%) are obtained, indicative of insufficient ability of polysulfides blocking. To further pursue high-energy-density Li-S batteries, the S/CNT cathode that with 79 wt% sulfur content (Figure S31, Supporting Information) was prepared and used to study the electrochemical performances with high-sulfur loading (≥5 mg cm⁻²) and lean electrolyte (5 μL mg^s⁻¹). As shown in Figure 5d, the SCOF-2 modified cells with 3.2,

5.3, and 8.2 mg cm⁻² show initial capacities of 1036, 916, and 740 mAh g⁻¹ after two cycles of preactivation at 0.05 C, and maintain 855, 698, and 601 mAh g⁻¹ after 100 cycles at the current of 0.2, 0.15, and 0.1 C, respectively, accompanying with 82.5%, 76.2%, and 81.2% capacity retentions (Figure S32, Supporting Information). Accordingly, the SCOF-2 modified cell can reach an areal capacity of 6.06 mAh cm⁻² and retain a desirable capacity of 4.92 mAh cm⁻² after 100 cycles, which is superior to the state-of-the-art LIBs (≈4 mAh cm⁻²) and overwhelms most other organosulfur cathodes or polymer-modified separators used in Li–S field (Tables S1 and S2, Supporting Information).

3. Conclusion

In summary, we design and synthesize a sulfonate-rich COF (SCOF-2) and use it to modify the separator of Li–S batteries, providing a solution for tackling the issues of polysulfides shuttle and Li-dendrite growth. In comparison with the none/monosulfonate COFs, the dual-sulfonated COF (SCOF-2) with concentrated negative charge holds the merits of enhanced interlayer spacing and narrow bandgap, which can not only facilitate the Li⁺ migration but also alleviate the formation of Li-dendrites. Moreover, the SCOF-2 could block polysulfides via both electrostatic repulsion (i.e., repelling polysulfide anions) and chemical trapping (i.e., adsorbing molecular LiPSs). Therefore, the SCOF-2 modified cells exhibit excellent anti-self-discharge behavior by a low capacity attenuation of 6.0% over one week rest, and an ultralow attenuation rate of 0.047% per cycle over 800 cycles at 1 C. When coupled with S/CNT cathode under the conditions of 8.2 mg cm⁻² sulfur loading and lean electrolyte (5 μL mg^s⁻¹), a desirable reversible capacity of 4.92 mAh cm⁻² and 81.2% capacity retention over 100 cycles were achieved. This work may evoke the enthusiasm for exploring advanced COFs for high-performance Li–S batteries.

Supporting Information

Supporting Information is available from the Wiley Online Library or from the author.

Acknowledgements

J.X. and S.A. contributed equally to this work. The authors acknowledge funding support from the National Key Research and Development Program of China (2018YFE0201702), the National Natural Science Foundation of China (21975052, 21935003, 21805126), and the China Postdoctoral Science Foundation (Nos. 2021M690662, 2019M661408).

Note: In the initially published version, the data used for the inset of Figure S17b, Supporting Information, which shows EIS plots of the Celgard sample, was the data for the SCOF-1 sample, which had already been displayed in Figure S16b. The figure was corrected in the Supporting Information file on December 7, 2021. As a consequence of the error, the originally reported value for the Li⁺ transference number of the pristine Celgard separator, in the left column of page 4 (paragraph 4 of Section 2), was also incorrect. This was also corrected on December 7, 2021, to 0.61. Raw data pertaining to the correction of these errors are available from the corresponding author upon reasonable request.

Conflict of Interest

The authors declare no conflict of interest.

Data Availability Statement

The data that support the findings of this study are available from the corresponding author upon reasonable request.

Keywords

covalent organic frameworks, Li–S batteries, modified separators, shuttle inhibition, dendrite-free batteries

Received: July 6, 2021
Revised: August 23, 2021
Published online: October 7, 2021

- [1] a) B. Dunn, H. Kamath, J.-M. Tarascon, *Science* **2011**, *334*, 928; b) P. G. Bruce, S. A. Freunberger, L. J. Hardwick, J.-M. Tarascon, *Nat. Mater.* **2012**, *11*, 19; c) L. Ma, Y. Lv, J. Wu, C. Xia, Q. Kang, Y. Zhang, H. Liang, Z. Jin, *Nano Res.* **2021**, <https://doi.org/10.1007/s12274-021-3439-3>; d) C. Cui, C. Yang, N. Eidson, J. Chen, F. Han, L. Chen, C. Luo, P.-F. Wang, X. Fan, C. Wang, *Adv. Mater.* **2020**, *32*, 1906427.
- [2] a) Z. W. Seh, Y. Sun, Q. Zhang, Y. Cui, *Chem. Soc. Rev.* **2016**, *45*, 5605; b) H.-J. Peng, J.-Q. Huang, X.-B. Cheng, Q. Zhang, *Adv. Energy Mater.* **2017**, *7*, 1700260; c) Z. Zhuang, Q. Kang, D. Wang, Y. Li, *Nano Res.* **2020**, *13*, 1856; d) J. Wu, S. Liu, F. Han, X. Yao, C. Wang, *Adv. Mater.* **2021**, *33*, 2000751.
- [3] a) J. Zhang, C. P. Yang, Y. X. Yin, L. J. Wan, Y. G. Guo, *Adv. Mater.* **2016**, *28*, 9539; b) Y. Yao, H. Wang, H. Yang, S. Zeng, R. Xu, F. Liu, P. Shi, Y. Feng, K. Wang, W. Yang, X. Wu, W. Luo, Y. Yu, *Adv. Mater.* **2020**, *32*, 1905658; c) J. Wang, Y.-S. He, J. Yang, *Adv. Mater.* **2015**, *27*, 569; d) G. Hu, Z. Sun, C. Shi, R. Fang, J. Chen, P. Hou, C. Liu, H.-M. Cheng, F. Li, *Adv. Mater.* **2017**, *29*, 1603835.
- [4] a) P. Arora, Z. Zhang, *Chem. Rev.* **2004**, *104*, 4419; b) J.-Q. Huang, Q. Zhang, H.-J. Peng, X.-Y. Liu, W.-Z. Qian, F. Wei, *Energy Environ. Sci.* **2014**, *7*, 347; c) Y. Chen, Q. Kang, P. Jiang, X. Huang, *Nano Res.* **2021**, *14*, 2424.
- [5] a) Q. Pang, X. Liang, C. Y. Kwok, L. F. Nazar, *Nat. Energy* **2016**, *1*, 16132; b) A. Manthiram, Y. Fu, S.-H. Chung, C. Zu, Y.-S. Su, *Chem. Rev.* **2014**, *114*, 11751.
- [6] a) Y. He, Z. Chang, S. Wu, Y. Qiao, S. Bai, K. Jiang, P. He, H. Zhou, *Adv. Energy Mater.* **2018**, *8*, 1802130; b) J. Wang, J. Zhang, S. Cheng, J. Yang, Y. Xi, X. Hou, Q. Xiao, H. Lin, *Nano Lett.* **2021**, *21*, 3245.
- [7] a) Z. Cheng, H. Pan, H. Zhong, Z. Xiao, X. Li, R. Wang, *Adv. Funct. Mater.* **2018**, *28*, 1707597; b) T. Sun, J. Xie, W. Guo, D.-S. Li, Q. Zhang, *Adv. Energy Mater.* **2020**, 1904199, <https://doi.org/10.1002/aenm.201904199>; c) Z.-J. Zheng, H. Ye, Z.-P. Guo, *Energy Environ. Sci.* **2021**, *14*, 1835.
- [8] a) H. Liao, H. Ding, B. Li, X. Ai, C. Wang, *J. Mater. Chem. A* **2014**, *2*, 8854; b) Y. Meng, G. Lin, H. Ding, H. Liao, C. Wang, *J. Mater. Chem. A* **2018**, *6*, 17186.
- [9] a) S. H. Je, H. J. Kim, J. Kim, J. W. Choi, A. Coskun, *Adv. Funct. Mater.* **2017**, *27*, 1703947; b) F. Xu, S. Yang, G. Jiang, Q. Ye, B. Wei, H. Wang, *ACS Appl. Mater. Interfaces* **2017**, *9*, 37731.
- [10] a) Q. X. Shi, H. J. Pei, N. You, J. Wu, X. Xiang, Q. Xia, X. L. Xie, S. B. Jin, Y. S. Ye, *Chem. Eng. J.* **2019**, *375*, 121977; b) J.-Q. Huang, Q. Zhang, F. Wei, *Energy Storage Mater.* **2015**, *1*, 127; c) Y. Cao,

- H. Wu, G. Li, C. Liu, L. Cao, Y. Zhang, W. Bao, H. Wang, Y. Yao, S. Liu, F. Pan, Z. Jiang, J. Sun, *Nano Lett.* **2021**, 21, 2997; d) X. Deng, Y. Li, L. Li, S. Qiao, D. Lei, X. Shi, F. Zhang, *Nanotechnology* **2021**, 32, 275708.
- [11] a) C. Jiang, M. Tang, S. Zhu, J. Zhang, Y. Wu, Y. Chen, C. Xia, C. Wang, W. Hu, *Angew. Chem., Int. Ed.* **2018**, 57, 16072; b) R. Wang, Q. Cai, Y. Zhu, Z. Mi, W. Weng, Y. Liu, J. Wan, J. Hu, C. Wang, D. Yang, J. Guo, *Chem. Mater.* **2021**, 33, 3566.
- [12] Y. Cao, C. Liu, M. Wang, H. Yang, S. Liu, H. Wang, Z. Yang, F. Pan, Z. Jiang, J. Sun, *Energy Storage Mater.* **2020**, 29, 207.
- [13] J. Too, S.-J. Cho, G. Y. Jung, S. H. Kim, K.-H. Choi, J.-H. Kim, C. K. Lee, S. K. Kwak, S.-Y. Lee, *Nano Lett.* **2016**, 16, 3292.
- [14] a) K. Jeong, S. Park, G. Y. Jung, S. H. Kim, Y.-H. Lee, S. K. Kwak, S.-Y. Lee, *J. Am. Chem. Soc.* **2019**, 141, 5880; b) Y. Peng, G. Xu, Z. Hu, Y. Cheng, C. Chi, D. Yuan, H. Cheng, D. Zhao, *ACS Appl. Mater. Interfaces* **2016**, 8, 18505.
- [15] T.-Z. Hou, W.-T. Xu, X. Chen, H.-J. Peng, J.-Q. Huang, Q. Zhang, *Angew. Chem., Int. Ed.* **2017**, 56, 8178.
- [16] K. Kong, S. Zhang, Y. Chu, Y. Hu, F. Yu, H. Ye, H. Ding, J. Hua, *Chem. Commun.* **2019**, 55, 8090.
- [17] J. Xu, F. Yu, J. Hua, W. Tang, C. Yang, S. Hu, S. Zhao, X. Zhang, Z. Xin, D. Niu, *Chem. Eng. J.* **2019**, 123694, <https://doi.org/10.1016/j.cej.2019.123694>; b) L. Ma, P. Nath, Z. Tu, M. Tikekar, L. A. Archer, *Chem. Mater.* **2016**, 28, 5147.
- [18] a) W. Yao, W. Zheng, J. Xu, C. Tian, K. Han, W. Sun, S. Xiao, *ACS Nano* **2021**, 15, 7114; b) W. Yao, W. Zheng, K. Han, S. Xiao, *J. Mater. Chem. A* **2020**, 8, 19028.
- [19] J. Xu, W. Tang, F. Yu, S. Zhao, D. Niu, X. Zhang, Z. Xin, R. Chen, *J. Mater. Chem. A* **2020**, 8, 19001.
- [20] C. Zhao, G. Xu, Z. Yu, L. Zhang, I. Hwang, Y. Mo, Y. Ren, L. Cheng, C. Sun, Y. Ren, X. Zuo, J. Li, S. Sun, K. Amine, T. Zhao, *Nat. Nanotechnol.* **2020**, 16, 166.
- [21] J. Xu, S. Bi, W. Tang, Q. Kang, D. Niu, S. Hu, S. Zhao, L. Wang, Z. Xin, X. Zhang, *J. Mater. Chem. A* **2019**, 7, 18100.
- [22] S. Bai, X. Liu, K. Zhu, S. Wu, H. Zhou, *Nat. Energy* **2016**, 1, 16094.
- [23] a) T. Lei, W. Chen, W. Lv, J. Huang, J. Zhu, J. Chu, C. Yan, C. Wu, Y. Yan, W. He, J. Xiong, Y. Li, C. Yan, J. B. Goodenough, X. Duan, *Joule* **2018**, 2, 2091; b) C. Tian, B. Li, X. Hu, J. Wu, P. Li, X. Xiang, X. Zu, S. Li, *ACS Appl. Mater. Interfaces* **2021**, 13, 6229.
- [24] J. Xia, W. Hua, L. Wang, Y. Sun, C. Geng, C. Zhang, W. Wang, Y. Wan, Q.-H. Yang, *Adv. Funct. Mater.* **2021**, 31, 2101980.
- [25] C. Zhang, Y. Qiao, P. Xiong, W. Ma, P. Bai, X. Wang, Q. Li, J. Zhao, Y. Xu, Y. Chen, J. H. Zeng, F. Wang, Y. Xu, J. Jiang, *ACS Nano* **2019**, 13, 745.
- [26] a) Z. A. Ghazi, L. Zhu, H. Wang, A. Naeem, A. M. Khattak, B. Liang, N. A. Khan, Z. Wei, L. Li, Z. Tang, *Adv. Energy Mater.* **2016**, 6, 1601250; b) X. Ren, Q. Sun, Y. Zhu, W. Sun, Y. Li, L. Lu, *ACS Appl. Energy Mater.* **2020**, 3, 4023.
- [27] a) Z. Li, F. Zhang, T. Cao, L. Tang, Q. Xu, H. Liu, Y. Wang, *Adv. Funct. Mater.* **2020**, 30, 2006297; b) W. Cai, G. Li, K. Zhang, G. Xiao, C. Wang, K. Ye, Z. Chen, Y. Zhu, Y. Qian, *Adv. Funct. Mater.* **2018**, 28, 1704865.
- [28] a) A. Bhargav, J. He, A. Gupta, A. Manthiram, *Joule* **2020**, 4, 285; b) M. Zhao, B. Li, X. Zhang, J. Huang, Q. Zhang, *ACS Cent. Sci.* **2020**, 6, 1095.